Lab on a Chip

PAPER

View Article Online
View Journal | View Issue

Cite this: *Lab Chip*, 2022, **22**, 343

Hybrid skin chips for toxicological evaluation of chemical drugs and cosmetic compounds†

Jong Seung Lee,‡[a] Jin Kim,‡[a] Baofang Cui,[a] Su Kyeom Kim,[a] Sun-A Cho,[b] Susun An[b] and Seung-Woo Cho *[acd]

Received 21st June 2021,
Accepted 5th December 2021

DOI: 10.1039/d1lc00550b

rsc.li/loc

Development of drugs and cosmetics for topical application require safety tests in skin models. However, current skin models, such as skin cell sheets and artificial tissue-engineered skin, do not allow sophisticated toxicological evaluations (*e.g.*, sensory irritation, hepatotoxicity). Animal models are prohibited worldwide for testing cosmetics. Therefore, reliable human skin models that recapitulate physiological events in skin tissue need to be established under *in vitro* settings. In this study, hybrid human skin models that enable delicate toxicological evaluations of drugs and cosmetic compounds are demonstrated. To recapitulate skin cornification, keratinocytes in the top layer of a vertical microfluidic chip were cultured at the air–liquid interface. For the skin–nerve hybrid model, differentiated neural stem cells in 3D collagen were positioned adjacent to and right below the skin layer. This model enables real-time quantitative skin sensitization analysis following chemical treatments by detecting alterations in neuronal activity in combination with a calcium imaging technique. For the skin–liver model, hepatic cells derived from pluripotent stem cells were cultured in 3D collagen distant from the skin layer. Potential hepatotoxicity of cutaneously applied chemicals in this model can be evaluated by quantification of glutathione and reactive oxygen species. Our study suggests that 3D hybrid skin chips would provide useful human skin models in pharmaceutical and cosmetic industries.

Introduction

Toxicology tests of raw materials and chemicals are critical in the development of novel medicines and cosmetics. Because cutaneously applied drugs and cosmetics often evoke skin irritation and sensitization, as well as tissue damage caused by toxicity, these safety concerns need to be carefully considered before approval for application to humans.[1,2] In particular, given a worldwide prohibition of animal experiments for cosmetics, alternatives to animal testing are inevitable for developing cosmetics.[3,4] In recent decades, artificial skins have been widely utilized for drug screening and toxicological evaluation of drug candidates and cosmetic elements.[5–9] However, they have several limitations, including high cost due to complicated manufacturing processes and large batch-to-batch variation leading to low reproducibility.[10–12] To overcome those limitations of artificial skins, bioengineering techniques such as 3D bioprinting have been applied to construct *in vitro* skin model.[13–15] Skin chip models have also been established with microfluidic systems to model skin problems such as edema, psoriasis, skin cancer, and wounds, but most of the reported skin chips, which have relied on skin cells without epidermal cornification and without other non-cutaneous cell types, are quite unlike dynamic and complex natural skin environments.[16–21] Thus, current skin chips do not enable sophisticated evaluations such as sensitization and toxicity to internal organs.

In this study, we developed hybrid human skin models that recapitulate *in vivo*-like skin physiology and allow sophisticated toxicological evaluations, which have not been achieved with conventional artificial skin tissues or skin chips. Hybrid skin chips were fabricated with multichannel microfluidic devices containing compartments for different cell types. The skin layer with human keratinocytes in the top channel was exposed to air for cornification, and neuronal and hepatic cells derived from human stem cells were co-cultured in 3D hydrogel in different channels for the skin–

[a] *Department of Biotechnology, Yonsei University, Seoul 03722, Republic of Korea. E-mail: seungwoocho@yonsei.ac.kr*
[b] *Safety & Microbiology Lab, Amorepacific Co. R&D Unit, Yongin 17038, Republic of Korea*
[c] *Center for Nanomedicine, Institute for Basic Science (IBS), Seoul 03722, Republic of Korea*
[d] *Graduate Program of Nano Biomedical Engineering (NanoBME), Advanced Science Institute, Yonsei University, Seoul 03722, Republic of Korea*

† Electronic supplementary information (ESI) available. See DOI: 10.1039/d1lc00550b

‡ These authors contributed equally to this work.

nerve and skin–liver models, respectively. We confirmed the feasibility of these hybrid skin models for quantitative evaluation of sensitization and hepatotoxicity by treatment of chemical drugs and cosmetic compounds.

Results and discussion

Fabrication of microfluidic chips for hybrid skin models

Hybrid skin model chips were designed to co-culture multiple cell types in spatially compartmented sections, while allowing interconnectivity between different sections. One hybrid skin model unit in a microfluidic device made of poly(dimethylsiloxane) (PDMS) was fabricated to have microchannels for four major sections (Fig. 1A). Six units were arranged repetitively in one device to increase throughput in culture and analysis. For skin epidermis reconstitution, human keratinocytes were cultured as a monolayer in the top channel (1st section) (Fig. 1A and B). The keratinocyte layer was maintained at an air–liquid interface to induce cornification by aeration. For the skin–nerve hybrid model (Fig. 1B, top panel), human neural stem cells (hNSCs) were cultured within 3D collagen type I hydrogel matrix in the second channel (2nd section), right below the skin layer. For the skin–liver hybrid model (Fig. 1B, bottom panel), human induced pluripotent stem cell-derived hepatocyte-like cells (hiPSC-HEPs) were encapsulated within 3D collagen hydrogel in the third channel (3rd section), right above the medium supply channel (4th section). Empty channels in the skin–nerve and skin–liver models were filled with 3D collagen hydrogel alone, without cell encapsulation, in the third and second channels, respectively (Fig. 1B). The fabricated hybrid skin chip with six replicate units can be utilized compatibly with a regular multichannel pipette (Fig. 1C). Administration of hydrogels and cell seeding in multi-sections were carried out as illustrated in Fig. 2A.

We adopted different structural designs in the skin–nerve and skin–liver models to recapitulate *in vivo*-like situations for more accurate and sophisticated toxicological evaluations of drugs and cosmetic compounds. The skin–nerve hybrid model was designed to place the nerve part right below the skin layer without a hydrogel barrier to reconstitute the *in vivo* condition where nerve exists adjacent to the skin layer. The skin–liver hybrid model was designed to have a hydrogel barrier that separates the epidermal layer and the liver part. As chemicals applied to skin are not transferred directly to liver, we included an empty hydrogel layer between skin and liver channels to reconstitute such indirect molecular transfer under *in vivo* situation. Phenotypes and functions of cells applied for hybrid skin models were confirmed before use. Neuronal cells derived from hNSCs used for hybrid skin–nerve model showed expression of several neuronal markers (Tuj1, MAP2, NeuN) and electrophysiological responses to

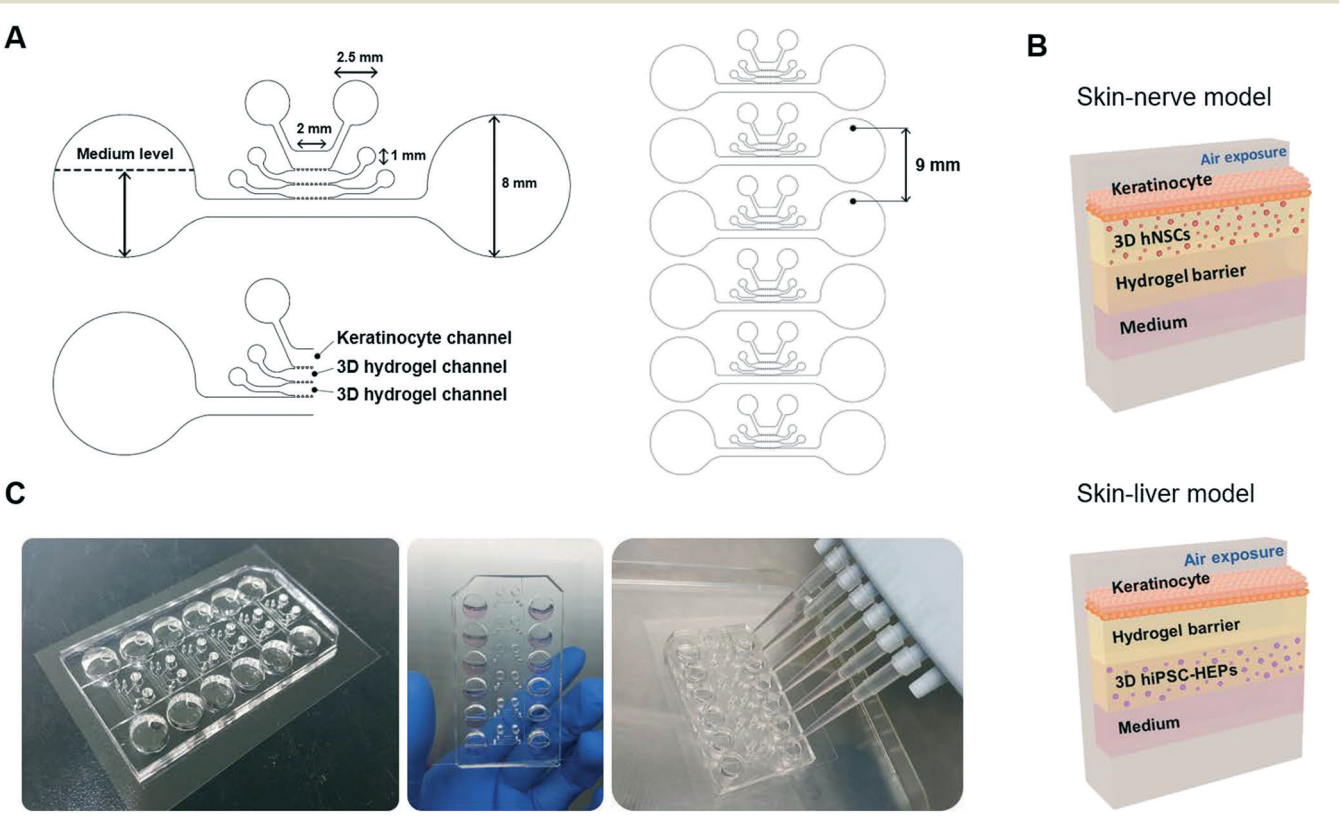

Fig. 1 Microfluidic chip design of hybrid skin models. (A) Design of a hybrid skin model unit and whole chip design with six parallel units. (B) Schematic of skin–nerve and skin–liver models. (C) Photos of fabricated hybrid skin chips.

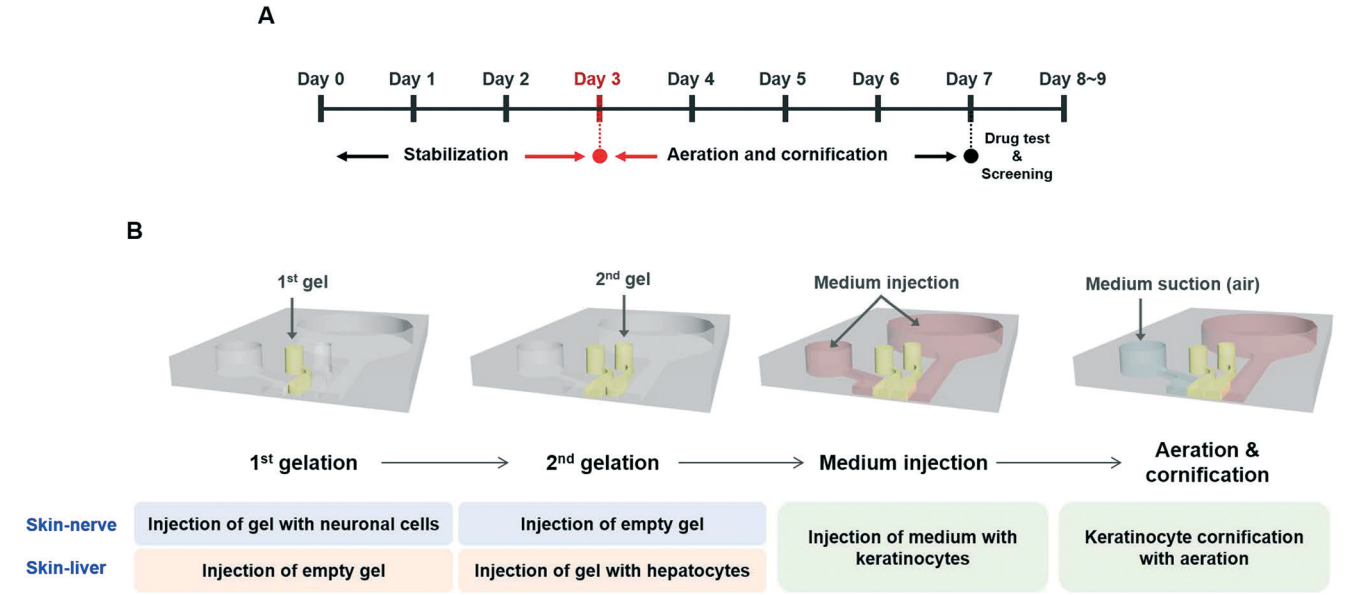

Fig. 2 Fabrication procedure for hybrid skin chips. (A) Timeline to construct hybrid skin chips (stabilization, aeration, and cornification) and test drugs. (B) Schematic of fabrication sequences for skin–nerve and skin–liver models. Serial gelation and cell seeding were conducted to construct hybrid skin models.

neurotransmitter glutamate (Fig. S1†), indicating their functional neuronal activity. Likewise, hiPSC-HEPs used for hybrid skin–liver model exhibited high expression of mature hepatic markers (HNF4A, albumin) and CYP3A4 activity (Fig. S2†), indicating maturation and hepatic functionality of hiPSC-HEPs. These characterization data support the functionality of neuronal and hepatic cells in our hybrid skin models.

Construction of hybrid skin models

Hybrid skin models were constructed through stabilization and aeration after cell seeding (Fig. 2B). To induce formation of a thick epidermis layer, seeded keratinocytes were stabilized in medium for three days. Then, medium in the top channel was removed, and the skin layer was cultured with exposure to air to induce cornification. This aeration

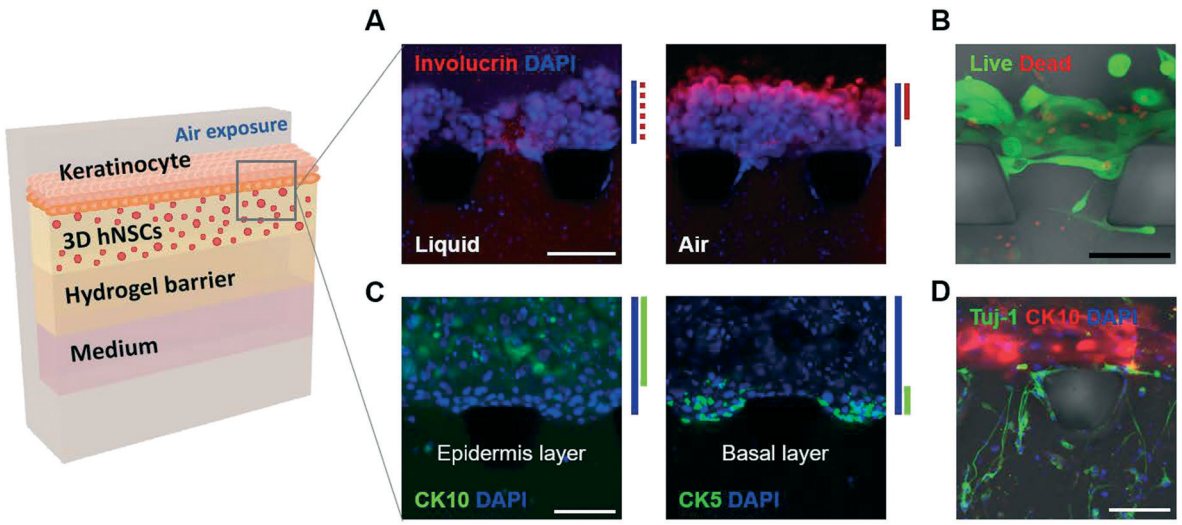

Fig. 3 Characterization of a microfluidic skin–nerve model. (A) Immunocytochemical staining of human keratinocyte-seeded skin layers, exposed to either medium or air, to detect involucrin. A tightly stacked skin layer with intensive expression of involucrin was formed only in the air-exposed condition. Scale bar = 200 μm. (B) LIVE/DEAD staining to check cell viability at day 1 after construction of the hybrid skin chip. Live cells were stained with calcein-AM in green, and dead cells were stained with ethidium homodimer in red. Scale bar = 200 μm. (C) Immunostaining of skin layers for epidermal (CK10) and basal (CK5) markers. Basal layer and epidermis layer were well organized in the skin layer exposed to air. Scale bar = 200 μm. (D) Immunocytochemical staining of neuronal cells differentiated from human neural stem cells (hNSCs) in 3D collagen hydrogel (2nd section) to detect the neuronal marker Tuj1 (green). CK10-positive epidermis layer (red) was shown in the skin channel (1st section). Scale bar = 200 μm.

process is critical for constructing a physical barrier for the skin layer. In air exposure conditions, the layered structure of skin epidermis was well maintained, with intensive involucrin expression on the top position (Fig. 3A). In contrast, skin layer cultured without air exposure did not develop an involucrin-expressing layer and tight barrier structures (Fig. 3A). As one precursor protein of the envelope of cornified cells, involucrin is important for function of the skin layer as a stable barrier.[22,23] Therefore, an aeration process to induce construction of cornified skin layer, including an involucrin-expressing layer, is required for accurate toxicity evaluation of topical medications and cosmetics. For co-culture of hybrid skin models, culture media for different type of cells were mixed. Keratinocyte and neuronal cell culture media were mixed in a 1 : 1 ratio for the skin–nerve model. Likewise, keratinocyte and hepatic cell culture media were mixed in 1 : 1 ratio for the skin–liver model. LIVE/DEAD staining assays indicated that cells in the skin–nerve hybrid model are highly viable during the culture (Fig. 3B). The reconstituted epidermis layer in the hybrid skin model showed overall expression of cytokeratin 10 (CK10), and a well-organized basal skin layer was observed that stained positively for cytokeratin 5 (CK5), which is expressed in basal keratinocytes in the stratified epithelium (Fig. 3C and S3†). Neuronal cells differentiated from encapsulated hNSCs were found to express the neuronal marker tubulin beta III (Tuj1) in 3D hydrogel in direct contact with the cornified skin layer, providing a 3D nerve component of the skin–nerve model (Fig. 3D). In the skin–liver model, hiPSC-HEPs expressing the hepatic marker albumin (ALB) were maintained in 3D hydrogel in indirect contact with the CK5-positive basal skin layer (Fig. 4A), and most hiPSC-HEPs retained high viability during co-culture (Fig. 4B).

Our hybrid skin model has several different features from previously demonstrated multi-channel chips with 3D hydrogel and air–liquid interface.[24,25] For establishing effective 3D hybrid skin models, we focused two detailed points distinct from conventional chip designs. First, we devised our chip for hybrid skin models comprising multiple cell types such that our chip can recapitulate better *in vivo* situations. The chips for previous skin models have only one 3D hydrogel channel, which limits the culture of multiple cell types in 3D. In contrast, our chip has unsymmetric post direction allowing serial injection into two parallel 3D hydrogel channels while reducing the possibility of air bubble trapping between posts at hydrogel intersection. Accordingly, cornified skin layer can be reconstituted in top channel and other tissue parts such as nerve and liver can also be properly placed in these 3D hydrogel channels. Therefore, our chip design would be more advantageous in preparing hybrid skin models with other tissue compartments. Second, we adapted vertical chip configuration for reliable air–liquid interface culture. To overcome the limitations of horizontally operating conventional chips in air–liquid interface culture, we designed chip configuration to be fitted for vertical operation and adjusted the positions of medium reservoirs to secure air exposure in the skin channel. Consequently, the upper region of the skin layer in the top channel can be stably exposed to air and the bottom of the skin layer can be supplied with medium through next 3D hydrogel channel, leading to reconstitution of *in vivo*-like skin structure with cornified layer and basal layer. Overall, our chip design with modified configuration and compartments enables establishment of an advanced *in vitro* hybrid skin model.

Drug response of cornified skin layer in the hybrid skin model

To prove the ability of the developed hybrid skin models to evaluate drug toxicity, tretinoin, a representative chemical to

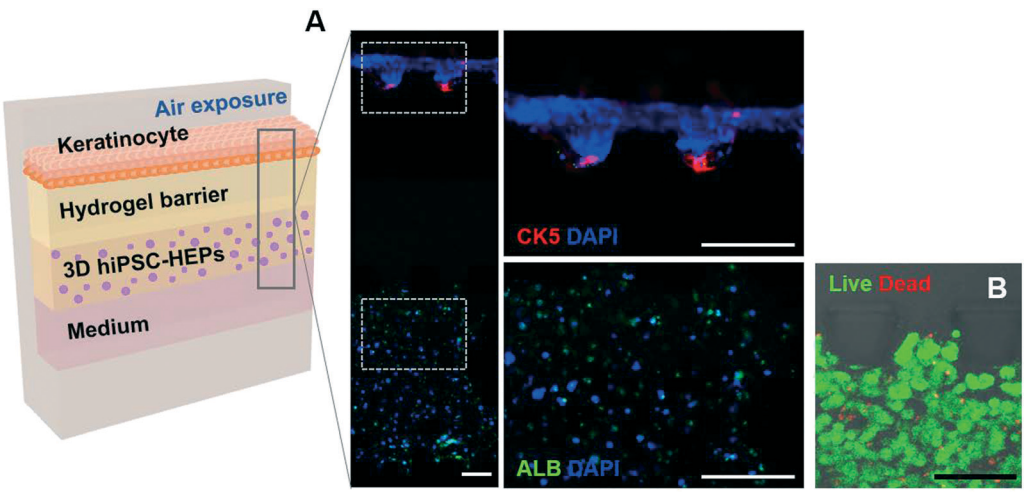

Fig. 4 Characterization of a microfluidic skin–liver model. (A) Immunocytochemical staining of human induced pluripotent stem cell-derived hepatocyte-like cells (hiPSC-HEPs) in 3D collagen hydrogel (3rd section) to detect the hepatic marker ALB (green). CK5-positive basal layer (red) was shown in the skin channel (1st section). Scale bars = 200 μm. (B) LIVE/DEAD staining to check the viability of hiPSC-HEPs (in the 3rd section) at day 1 after construction of the hybrid skin chip. Scale bar = 200 μm.

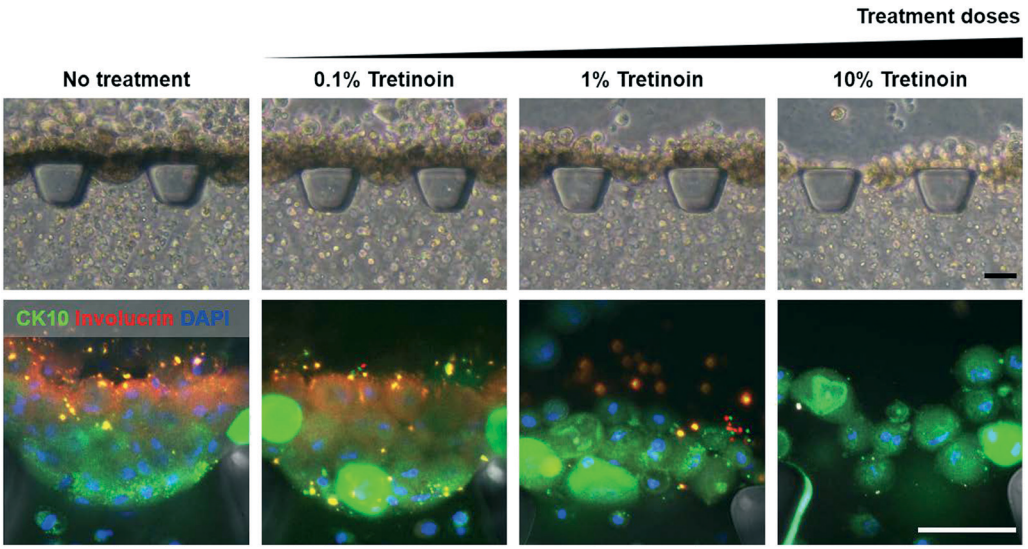

Fig. 5 Exfoliation test of hybrid skin chips. Exfoliation of cornified keratinocytes in the skin layer was induced by tretinoin treatment, which is known to exfoliate dead skin cells. The dose of tretinoin normally used for cosmetic and medical purposes is 0.1% (w/v). Microscopic observation (top rows) and immunocytochemical staining for epidermis markers (CK10, involucrin; bottom rows) in the skin layer 48 hours after tretinoin treatment indicated exfoliation of cornified epidermis in the hybrid skin chip. The epidermal layer became thinner upon treatment with tretinoin, and the skin layer exposed to excessive doses collapsed. Scale bars = 100 μm.

be applied to skin, was administered onto the top layer of reconstituted epidermis in the skin–nerve model (Fig. 5). Tretinoin is widely used for cosmetic and medical purposes to exfoliate dead skin cells. This chemical is generally administrated in a dose of 0.1% for exfoliation, but larger doses have been known to induce excessive skin damage.[26–28] Therefore, tretinoin was applied to the skin layer at doses of 0.1%, 1%, and 10% (Fig. 5). When the hybrid skin model was treated with a normal dose (0.1%) of tretinoin, overall skin layer structure was maintained, but the involucrin-expressing layer became slightly thinner than in the untreated group. In hybrid models treated with excessive doses (1%, 10%), skin layer structure collapsed and the involucrin-expressing layer disappeared, indicating complete exfoliation. These results demonstrate that the hybrid skin model exhibits drug responses similar to native skin, representing the possibility of our model as an alternative platform for testing cosmetics and chemical drugs targeting skin diseases.

Evaluation of skin sensitization with the hybrid skin–nerve model

Cutaneously applied chemicals often cause skin irritation by stimulating neuronal activity in skin tissue. Thus, abnormal neural excitation by chemical drugs and cosmetic compounds should be checked.[29–31] We examined the potential of our hybrid skin–nerve model to enable quantitative evaluation of skin irritation by chemicals as an alternative to conventional skin sensitization tests. To quantify the degree of skin sensitization following chemical treatments, a calcium imaging technique was combined with our hybrid model platform. The activity of neuronal cells treated with chemicals in the 3D nerve component was measured in real time by recording changes in intracellular calcium levels using the calcium-sensitive indicator Fluo-4 AM (Fig. 6A).

First, neuronal excitation in the hybrid skin–nerve model was tested with the well-known excitatory chemical capsaicin at concentrations ranging from 200 μM to 400 μM (Fig. 6B and C). We chose capsaicin as a testing chemical compound because it is one of the components commonly used in cosmetic products.[32–34] Treatment of the skin with capsaicin is known to increase circulation, improve tone and firmness, and induce vasodilation, which are great advantages in cosmetic industry.[35,36] Capsaicin is also known to have a potential to stimulate neuronal reactivity.[37] Capsaicin applied from outside the skin layer diffused through the skin layer to the adjacent 3D nerve channel and stimulated neuronal cells in a dose-dependent manner. The untreated group did not show a change in calcium influx. In contrast, intensity of calcium influx spikes and frequency of multi-spikes, which represent neuronal activity, increased in proportion to an increasing concentration of capsaicin (Fig. 6B and C).

Additionally, we tested other chemicals that stimulate neuronal activity or inhibit neuronal activation in the hybrid skin–nerve model (Fig. 6D). Lactic acid, which is widely used as an anti-wrinkle and pigmentation-fighting ingredient of skin care products, and strontium chloride, known as an inhibitor of sensory irritation, were applied for neural excitation and inhibition of neural excitation, respectively.[38–40] Neuronal cells in the 3D nerve channel responded actively to lactic acid, but the cells treated with strontium chloride were not activated (Fig. 6D). Interestingly, co-treatment with lactic acid and strontium chloride at the same time suppressed neuronal activation by lactic acid.

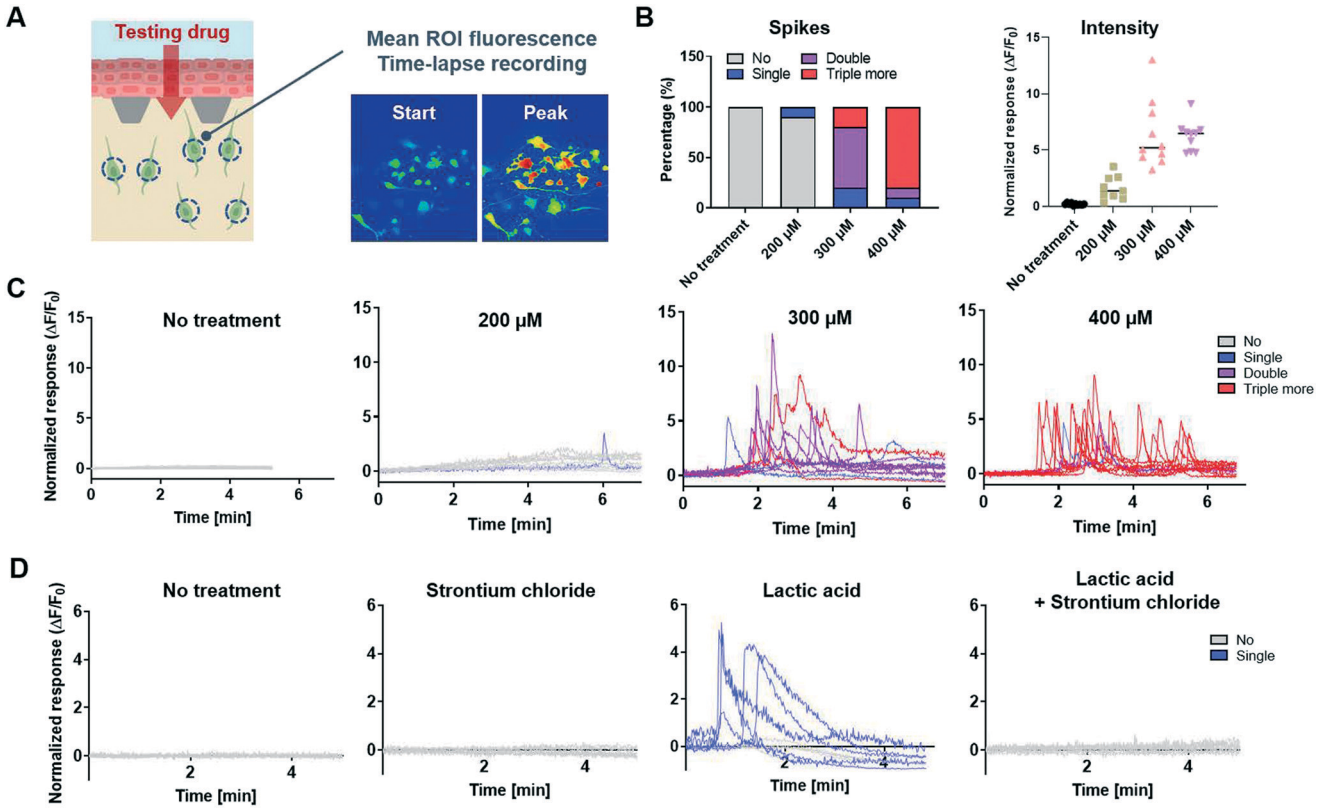

Fig. 6 Evaluation of neuronal reactivity in the skin–nerve model with calcium influx imaging. (A) Schematic of neuronal reactivity test with calcium imaging in the skin–nerve chip treated with drugs. Time-lapse changes in intracellular calcium levels of hNSC-derived neuronal cells were recorded with the calcium indicator Fluo-4. (B) The frequency of multi-spikes and the average intensity of calcium influx spikes, which were quantified with calcium imaging immediately after administration of a neuronal excitatory chemical (capsaicin) into the hybrid skin–nerve model. (C) Time-course of changes in intracellular calcium levels after treatment with capsaicin at different doses. Intracellular calcium level changes were recorded, and normalized to initial fluorescence intensity. (D) Time-course of responses of neuronal cells in the skin–nerve model when treated with a neuronal excitatory chemical (lactic acid) and a sensory relieving chemical (strontium chloride). Treatment with strontium chloride eliminated neuronal reactivity stimulated by lactic acid.

Collectively, these results demonstrate the feasibility of our hybrid skin–nerve model to monitor skin sensitization and sensory irritation following cutaneous application of chemical drugs and cosmetic compounds.

Evaluation of hepatotoxicity with the hybrid skin–liver model

Hepatotoxicity of chemical drugs often needs to be carefully examined, whether in the case of topical application or systemic administration.[41–44] Thus, we tested the hybrid skin–liver model for checking potential hepatotoxicity of chemical drugs. We chose acetaminophen and camphor as testing chemicals in the skin–liver hybrid model. Acetaminophen is the most widely used analgesic–antipyretic medication in the world. The most common formulation of this drug is a tablet for oral administration; however, other formulations, such as transdermal analgesic patch, have also been continuously tested.[42,45] Camphor, another chemical compound tested in the skin–liver model, is a naturally occurring compound derived from the wood of the camphor tree which has been used in both pharmaceutic and cosmetic industries.[46–49] Camphor has been used for a wide variety of topical applications in medical and cosmetic fields.[50,51] Owing to its pain-relieving and wound healing properties, camphor has been used for medical treatments. In addition, its ability to increase elastin and collagen production allows the usage as an ingredient of cosmetics. However, as acetaminophen and camphor are known to cause a hepatotoxicity,[52,53] potential hepatotoxicity of these chemicals following transdermal applications needs to be checked, which has not been carefully investigated yet.

Hepatotoxic chemical drugs (acetaminophen, camphor) applied to the outside of the skin layer diffused through the skin layer and adjacent 3D empty collagen hydrogel to the 3D liver channel (Fig. 7A and D). In hiPSC-HEPs treated with acetaminophen at different concentrations (0, 5, 10 mM), hepatotoxicity was evaluated by checking the levels of glutathione (GSH) and reactive oxygen species (ROS), which are key indicators of hepatotoxicity, using staining assays with monochlorobimane (mBCI) and dihydroethidium (DHE), respectively. GSH, one of the important molecules for detoxification, is vital for liver health.[54] One of the main pathways of detoxification occurs through conjugation with GSH, which facilitates elimination of poisons and toxins in

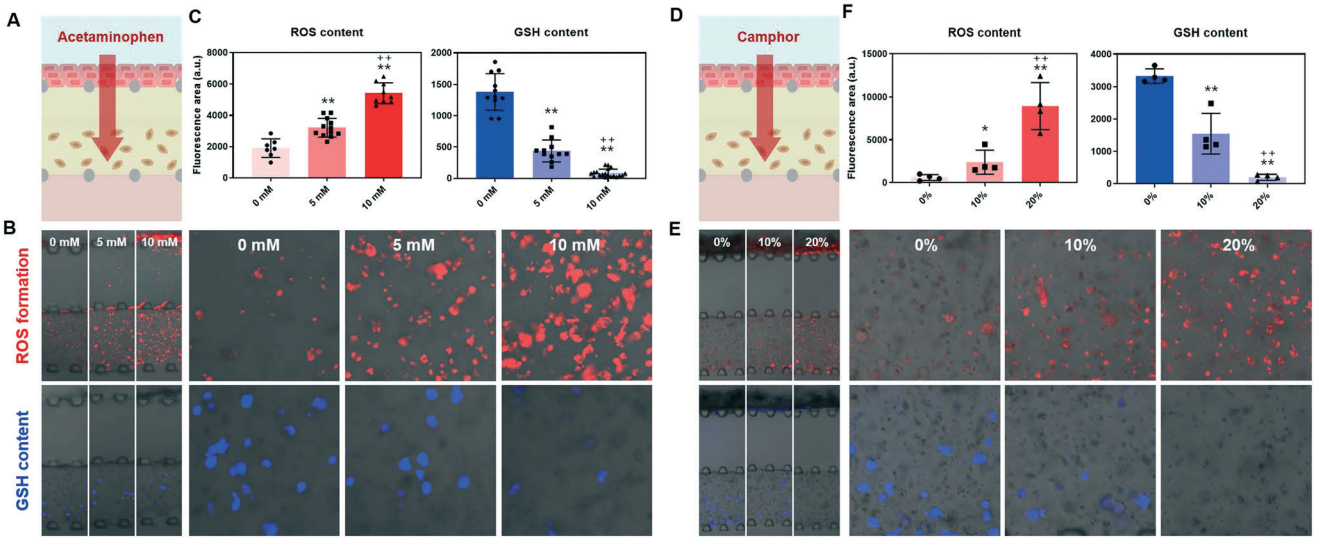

Fig. 7 Evaluation of hepatotoxicity in the skin–liver model. (A) Schematic illustration of acetaminophen treatment in the skin–liver chip. (B) ROS content stained with dihydroethidium and GSH content with monochlorobimane in hiPSC-HEPs in the skin–liver chip, 24 hours after treatment with acetaminophen at different doses (0, 5, and 10 mM). (C) Quantification of fluorescence area based on ROS- and GSH-stained images. As the dose of acetaminophen increased, ROS content was increased and GSH content was reduced (n = 7 to 19, $^{**}p < 0.01$ *vs.* 0 mM group, $^{++}p < 0.01$ *vs.* 5 mM group). (D) Schematic of camphor treatment in the skin–liver chip. (E) Images of ROS and GSH staining after 24 hours of camphor treatment at different concentrations (0%, 10%, and 20%, v/v). (F) Quantification of fluorescence area based on ROS- and GSH-stained images. Likewise, increasing doses of camphor increased ROS content but reduced GSH content (n = 4, $^{*}p < 0.05$, $^{**}p < 0.01$ *vs.* 0% group, $^{++}p < 0.01$ *vs.* 10% group).

the body.[55] Under conditions with high levels of toxins, the active form of GSH is rapidly exhausted during the detoxification process, and damaged hepatic cells release ROS.[56–60] As expected, GSH contents were reduced, and the level of ROS increased at higher dosages of acetaminophen (Fig. 7B and C). Likewise, the level of GSH decreased and the level of ROS increased in response to increasing camphor concentrations of 0%, 10%, and 20% (v/v) (Fig. 7E and F). Taken together, these results demonstrate that the hybrid skin–liver model allows toxicological assessment and efficient screening of chemical drugs that need to be applied through skin.

As the functions of skin barrier have already been well described in previous reports,[61,62] the skin layer in our skin–liver model was also expected to play an important role in blocking topically applied materials including drugs, cosmetic compounds, and pollutions. Since hiPSC-HEPs in the monoculture model without skin barrier are directly exposed to acetaminophen and camphor, the effects of chemical treatment on alteration in ROS and GSH contents are likely to be more significant and exaggerated in the monoculture model than in the skin–liver model with skin layer. Thus, monoculture model may not be able to replicate precise responses of hiPSC-HEPs to the drugs treated through the skin.

Our hybrid skin chip models show several advantages as multi-organ chip models. Integrated skin- and liver-chip models with co-culture system were previously demonstrated (*e.g.*, Chip2).[63,64] The chip with reconstructed epidermis part with human skin cells and liver part with hepatic cells has been used for investigating toxicity and pharmacokinetic and pharmacodynamic properties of chemicals administered *via* topical route. An on-chip micropump system with HUMIMIC Starter facilitates the establishment of 'Chip2' model without additional syringe pump and nozzles. Moreover, this chip system comprising two different organ models integrated with microfluidic channels enables accurate prediction of biodistribution and metabolism of various substances *in vivo*. The 'Chip2' model is an undoubtedly excellent system to evaluate multi-organ effects of the molecules, however it requires an extra controller to create circulation inside the chip that connects two different organ models. In addition, the number of pressure connectors of the controller may limit a throughput in the screening. On the other hand, our hybrid skin models can be established with high interconnectivity between multi-organ parts without additional controller and apparatus by serially arranging skin layer and other 3D tissue channels (nerve, liver) in a single chip unit. Additionally, our chip with multiple units in parallel is compatible with the use of multichannel pipettes for convenient use and easy handling. Thus, our hybrid skin chip model would be more beneficial to increase a throughput in chip setting and analysis.

Conclusions

Here, we report the development of novel hybrid human skin chips capable of circumventing limitations of conventional artificial skin and animal models. Hybrid skin models with cornified epidermis could be prepared *via* air–liquid interface

culture of skin cells and spatial compartmentalization of non-cutaneous components, including neuronal and hepatic lineage cells. The developed hybrid skin–nerve and skin–liver models could be readily integrated with representative analytical methods, such as calcium imaging for neuronal activity and GSH/ROS assays for hepatotoxicity. These integrated platforms of hybrid skin models facilitate quantitative evaluation of toxicological effects of cutaneously applied chemicals, such as sensitization, irritation, and hepatotoxicity, which have not been easily analyzed with conventional *in vitro* skin models and animals. In the future, the utility of our hybrid platform would be expanded to other physiological events, side effects, and diseases through hybridization with other cell types, such as immune cells, melanocytes, and hair follicle dermal papilla cells, among others.

Materials and methods

Fabrication of a microfluidic device for skin chips

The microfluidic device was fabricated using PDMS (Sylgard 184, Dow Corning, Midland, MI, USA) by a standard soft lithography process as previously described. Liquid PDMS was mixed with a curing agent at 1 : 10 (w/w) and poured onto a silicon wafer to cast thick PDMS layers featuring each microchannel for the hybrid skin model. To remove bubbles in PDMS, the mold was degassed in a vacuum chamber for at least 10 minutes. After the degassing step, PDMS was cured in a drying oven at 70 °C for 4 hours. Then, the PDMS body was cut and peeled from the mold. The PDMS body with microfluidic channels and glass coverslip were sterilized in an autoclave and by ultraviolet light overnight and then assembled into the chip device. Surface plasma treatment (CUTE; Femto Science, Seoul, Korea) was applied to bond the device parts. The assembled devices were then placed in a drying oven at 70 °C.

Culture of human neural stem cells

Culture of hNSCs was conducted as described in our previous study.[65] Prof. Kook In Park at Yonsei University College of Medicine kindly provided hNSCs, and the use of hNSCs was approved by the research ethics committee of Yonsei University College of Medicine (protocol #4-2003-0078). The hNSCs were cultured in Dulbecco's modified Eagle's medium/nutrient mixture F-12 (DMEM/F12) medium (GIBCO, Gaithersburg, MD, USA) with N-2 supplement (GIBCO) and penicillin–streptomycin (200 U ml^{-1}, GIBCO) in humidified air with 5% CO_2 at 37 °C. To maintain hNSCs, mitogenic factors, including basic fibroblast growth factor (20 ng ml^{-1}, Peprotech, Rocky Hill, NJ, USA), leukemia inhibitory factor (10 ng ml^{-1}, Merck Millipore, Burlington, MA, USA), and heparin (8 μg ml^{-1}, Merck Millipore), were added to the medium. To induce spontaneous differentiation, hNSCs were cultured in medium depleted of mitogenic factors. Neuronal phenotypes and functions of hNSC-derived neuronal cells were confirmed with immunostaining for several neuronal markers (Tuj1, MAP2, NeuN) and calcium influx imaging analysis.

Culture of human epidermal keratinocytes

Human epidermal keratinocytes (HEKs) were purchased from GIBCO. The HEKs were cultured in EpiLife™ medium (GIBCO) with human keratinocyte growth supplement (HKGS, GIBCO). For expansion, the HEKs were maintained in humidified air with 5% CO_2 at 37 °C.

Culture of human iPSC-derived hepatocyte-like cells

hiPSCs were maintained as described in our previous studies.[66,67] For hepatic differentiation, cells were first dissociated into single cells and definitive endoderm differentiation was induced. Roswell Park Memorial Institute (RPMI)-1640 medium (GIBCO) containing activin A (100 ng ml^{-1}, R&D Systems, Minneapolis, MN, USA) and CHIR99021 (2 μM, LC Laboratory, Woburn, MA, USA) was used for the first 1.5 days. These cells were further differentiated in the same culture medium with 100 ng ml^{-1} activin A, sodium butyrate (1 mM, Merck Millipore), and fetal bovine serum (0.2%, GIBCO) for the next 1.5 days. These definitive endoderm cells enter the hepatic endoderm stage for an additional 8 days. For the first 2 days, cells were treated with RPMI medium containing B-27 supplement (GIBCO), bone morphogenetic protein (20 ng ml^{-1}, Peprotech), and fibroblast growth factor 4 (FGF4; 30 ng ml^{-1}, R&D Systems), followed by treatment with B-27 supplement and retinoic acid (2 μM, Merck Millipore) in DMEM/F12 for 2 days. For an additional 4 days, cells were cultured with DMEM/F12 in the presence of B-27 supplement, nicotinamide (10 mM, Merck Millipore), bFGF (1 ng ml^{-1}), and ascorbic acid (100 μM, Merck Millipore) to induce hepatic endoderm. These hepatic endoderm cells were dissociated with TrypLE Express (GIBCO), and plated onto collagen type I-coated dishes for further maturation. For maturation to hepatocyte-like cells, hepatic endoderm cells were differentiated with hepatocyte culture medium (HCM; Lonza, Basel, Switzerland) containing hepatocyte growth factor (HGF; 20 ng ml^{-1}, Peprotech), B-27 supplement, and insulin-transferrin-selenium (ITS-X; Merck Millipore) for 4 days. For the next 4 days, cells were further cultured in the same medium containing oncostatin M (OSM; 20 ng ml^{-1}, ProSpec, Ness-Ziona, Israel) and dexamethasone (DEX; 10^{-6} M, Merck Millipore). Cells were cultured in humidified air with 5% CO_2 at 37 °C. Hepatic phenotypes and functions of hiPSC-HEPs were confirmed with immunostaining for several hepatic markers (HNF4A, ALB) and measurement of CYP3A4 activity (P450-Glo CYP3A4 Assay System, Promega, Madison, WI, USA).

Preparation of hybrid skin models

For hybrid skin models, multi-sections in the microfluidic device were constructed with a series of gelation and cell seeding. First, the 2nd section of the hybrid skin chip was filled with 3D collagen type I hydrogel (3 mg ml^{-1} of

final concentration, neutralized with NaOH, Corning Inc., Corning, NY, USA). For skin–nerve model, collagen solution containing hNSCs at a density of 1×10^4 cells per μl was administered into the second channel (2nd section). For the skin–liver model, collagen solution without cells was administered into the 2nd section. The hybrid skin chips were then incubated for gelation at 37 °C for 20 min. After gelation of the 2nd section, the third channel (3rd section) of the hybrid skin chip was filled with 3D collagen hydrogel. Empty collagen solution without cells was added for the skin–nerve model, while collagen solution containing hiPSC-derived hepatic endoderm cells at a density of 5×10^3 cells per μl was administered into the 3rd section for the skin–liver model. The hybrid skin chips were incubated again for gelation at 37 °C for 30 min. For gelation in both the 2nd and the 3rd sections, 3 to 5 μl collagen solution was added into the channels. After gelation, culture medium was supplied into the chips through the fourth channel (4th section), and keratinocytes were seeded in the first channel (1st section) at a density of 5×10^4 cells per chip. After 3 days for stabilization, medium in the 1st section was removed for aeration to induce cornification of the keratinocytes. The hybrid skin–nerve chips were maintained under the condition of a 1 : 1 mixture of hNSC medium (DMEM/F12 medium with N-2 supplement and penicillin–streptomycin) and HEK medium (EpiLife™ medium with HKGS). The hybrid skin–liver chips were cultivated with a 1 : 1 mixture of HEK medium (EpiLife™ medium with HKGS) and hiPSC-HEP medium (HCM medium with HGF, B-27, and ITS-X for the first 4 days, and HCM medium further containing OSM and DEX for the next 4 days).

Cell viability assay

In hybrid skin chips, a cell viability assay was performed at day 1 with the LIVE/DEAD viability kit (Invitrogen, Carlsbad, CA, USA). In the skin–nerve model, keratinocytes in the skin layer and hNSCs in the neuronal layer were stained with the kit. In the skin–liver model, hiPSC-HEPs in the hepatic layer were analyzed. In this assay, live cells are stained green with calcein-AM, and nuclei of the dead cells are stained red with ethidium homodimer.

Immunocytochemistry

Immunocytochemical staining was performed as previously described.[68] Cells were fixed with formalin solution (10%, Merck Millipore) for 30 min and then permeabilized with 0.05% (v/v) Triton X-100 (Merck Millipore) for 30 min. After blocking with goat serum (2%, GIBCO) for 1 hour, the samples were incubated with primary antibodies overnight at 4 °C. The following antibodies were used for staining: anti-involucrin (1 : 100, Abcam, Cambridge, UK), anti-cytokeratin 10 (1 : 150, Abcam), anti-cytokeratin 5 (1 : 150, Abcam), anti-Tuj1 (1 : 150, Cell Signaling Technology, Danvers, MA, USA), anti-ALB (1 : 150, Merck Millipore), anti-MAP2 (1 : 200, Cell Signaling Technology), anti-NeuN (1 : 200, Cell Signaling Technology), anti-HNF4A (1 : 200, Santa Cruz Biotechnology, Dallas, TX, USA), and anti-ZO-1 (1 : 100, Invitrogen). After washing with phosphate-buffered saline (PBS, Merck Millipore) for 1 day at 4 °C, samples were treated with secondary antibodies overnight at 4 °C. The following secondary antibodies were used for staining: Alexa Fluor 488 goat anti-mouse IgG (1 : 200, Invitrogen), Alexa Fluor 488 goat anti-rabbit IgG (1 : 200, Invitrogen), and Alexa Fluor 594 goat anti-rabbit IgG (1 : 200, Invitrogen). Cell nuclei were counterstained with 4′,6-diamidino-2-phenylindole (DAPI; 5 μg ml^{-1}, TCI, Tokyo, Japan) for 30 min at room temperature. The fluorescently stained signals were observed with a confocal microscope (LSM 880, Carl Zeiss, Oberkochen, Germany).

Skin exfoliation assay

To validate the feasibility of hybrid skin chips as a skin drug test platform, a well-known skin exfoliating chemical, tretinoin (Merck Millipore), was added onto the cornified keratinocyte layer. The skin layer was exposed to various concentrations of tretinoin ranging from the normal dosage of 0.1% to excessive dosages (1%, 10%), for 48 hours. Exfoliation of the skin layer was visualized using an optical microscope (IX73, Olympus, Tokyo, Japan) and confirmed through immunocytochemical staining for cytokeratin 10 (CK10) and involucrin.

Measurement of neural activity with calcium imaging

To validate the ability of the skin–nerve model as a sensitization test platform, activation of hNSC-derived neuronal cells in the 3D nerve channel following chemical treatments was analyzed with calcium imaging. Cells were treated with Fluo-4 AM dye (Invitrogen) for 30 min at 37 °C and washed two times with PBS before recording. Time-lapse changes in calcium levels in neuronal cells were imaged using a confocal microscope (Carl Zeiss) immediately after neuronal excitatory and inhibitory chemical treatments. For neural excitation, capsaicin (Merck Millipore) and lactic acid (Merck Millipore) were applied onto the outside of the skin layer. For inhibition of neural activity, strontium chloride (Merck Millipore) was loaded onto the skin layer.

Hepatotoxicity evaluation

To validate the ability of the skin–liver model as a toxicity test platform, chemical drugs with well-known hepatic toxicity, including acetaminophen (Merck Millipore) and camphor (Merck Millipore), were added onto the outside of the skin layer. After 24 hours of treatment, levels of GSH and ROS in hiPSC-HEPs in the 3D liver channel were measured using the fluorescent probes mBCI (5×10^{-6} M, Merck Millipore) and DHE (10^{-5} M, Merck Millipore), respectively. These probes were added into the hybrid skin chip for 30 min in the

incubator, and signals from each probe were detected by a confocal microscope.

Statistics

All data are presented as mean ± standard deviation. For statistical evaluation, a Student's *t*-test was applied to calculate statistical probability. Statistic calculation was performed using Prism 9 (GraphPad Software, San Diego, CA, USA). The statistical significance of the data was determined at 95% ($p < 0.05$) and 99% ($p < 0.01$) confidence intervals.

Author contributions

J. S. L., J. K., S.-A. C., S. A., and S.-W. C. conceptualized the project. J. K. and B. C. designed and fabricated the microfluidic chips. J. S. L. cultured keratinocytes and neural stem cells. S. K. K. provided stem cell-derived hepatocytes. J. S. L. and J. K. constructed hybrid skin chip models and conducted various analyses including immunostaining, cell viability assay, skin exfoliation assay, calcium imaging, and hepatotoxicity assay. J. S. L., J. K., and S.-W. C. wrote the manuscript. S.-W. C. supervised the project.

Conflicts of interest

J. S. L., J. K., S.-A. C., S. A., and S.-W. C. are inventors on a patent application related to this work (Korean Patent Pending 10-2020-0009543).

Acknowledgements

This work was supported by a grant (ORS04-01-17C202001) funded by AMOREPACIFIC within the AMOREPACIFIC Open Research program.

References

1 L. Semlin, M. Schafer-Korting, C. Borelli and H. C. Korting, *Drug Discovery Today*, 2011, **16**, 132–139.
2 C. R. Harington, *Nature*, 1947, **159**, 319–320.
3 B. E. Rollin, *Toxicol. Pathol.*, 2003, **31**(Suppl), 128–131.
4 M. Balls, *Lab. Anim.*, 1994, **28**, 193–211.
5 S. MacNeil, *Nature*, 2007, **445**, 874–880.
6 A. Przekora, *Cell*, 2020, **9**, 1622.
7 F. Netzlaff, C. M. Lehr, P. W. Wertz and U. F. Schaefer, *Eur. J. Pharm. Biopharm.*, 2005, **60**, 167–178.
8 E. Chung, H. Choi, J. E. Lim and Y. Son, *Tissue Eng. Regener. Med.*, 2014, **11**, 87–92.
9 U. Park and K. Kim, *Biotechnol. Bioprocess Eng.*, 2017, **22**, 659–670.
10 J. T. Shores, A. Gabriel and S. Gupta, *Adv. Skin Wound Care*, 2007, **20**, 493–508.
11 M. Ponec, E. Boelsma, S. Gibbs and M. Mommaas, *Skin Pharmacol. Appl. Skin Physiol.*, 2002, **15**(Suppl 1), 4–17.
12 S. H. Lee and J. H. Sung, *Adv. Healthcare Mater.*, 2018, **7**, 1700419.
13 B. S. Kim, M. Ahn, W.-W. Cho, G. Gao, J. Jang and D.-W. Cho, *Biomaterials*, 2021, **272**, 120776.
14 B. S. Kim, W. W. Cho, G. Gao, M. Ahn, J. Kim and D. W. Cho, *Small Methods*, 2021, **5**, 2100072.
15 B. S. Kim, S. Das, J. Jang and D. W. Cho, *Chem. Rev.*, 2020, **120**, 10608–10661.
16 M. Wufuer, G. Lee, W. Hur, B. Jeon, B. J. Kim, T. H. Choi and S. Lee, *Sci. Rep.*, 2016, **6**, 37471.
17 X. Ren, A. E. Getschman, S. Hwang, B. F. Volkman, T. Klonisch, D. Levin, M. Zhao, S. Santos, S. Liu, J. Cheng and F. Lin, *Lab Chip*, 2021, **21**, 1527–1539.
18 A. Pavesi, G. Adriani, A. Tay, M. E. Warkiani, W. H. Yeap, S. C. Wong and R. D. Kamm, *Sci. Rep.*, 2016, **6**, 26584.
19 J. Li, L. Zhu, M. Zhang and F. Lin, *Biomicrofluidics*, 2012, **6**, 24121–2412113.
20 F. Lin, F. Baldessari, C. C. Gyenge, T. Sato, R. D. Chambers, J. G. Santiago and E. C. Butcher, *J. Immunol.*, 2008, **181**, 2465–2471.
21 J. Lim, E. Cho, K. Lee, Y. Choi, Y. Seo, H. Jeon and J. Choi, *BioChip J.*, 2019, **13**, 105–114.
22 E. Candi, R. Schmidt and G. Melino, *Nat. Rev. Mol. Cell Biol.*, 2005, **6**, 328–340.
23 M. E. Mathyer, E. A. Brettmann, A. D. Schmidt, Z. A. Goodwin, I. Y. Oh, A. M. Quiggle, E. Tycksen, N. Ramakrishnan, S. J. Matkovich, E. Guttman-Yassky, J. R. Edwards and C. de Guzman Strong, *Nat. Commun.*, 2021, **12**, 2557.
24 A. R. Aref, M. Campisi, E. Ivanova, A. Portell, D. Larios, B. P. Piel, N. Mathur, C. Zhou, R. V. Coakley, A. Bartels, M. Bowden, Z. Herbert, S. Hill, S. Gilhooley, J. Carter, I. Canadas, T. C. Thai, S. Kitajima, V. Chiono, C. P. Paweletz, D. A. Barbie, R. D. Kamm and R. W. Jenkins, *Lab Chip*, 2018, **18**, 3129–3143.
25 M. H. Rambol, E. Han and L. E. Niklason, *Tissue Eng., Part A*, 2020, **26**, 556–568.
26 C. K. Kimbrough-Green, C. E. Griffiths, L. J. Finkel, T. A. Hamilton, S. M. Bulengo-Ransby, C. N. Ellis and J. J. Voorhees, *Arch. Dermatol.*, 1994, **130**, 727–733.
27 J. S. Weiss, C. N. Ellis, J. T. Headington, T. Tincoff, T. A. Hamilton and J. J. Voorhees, *JAMA*, 1988, **259**, 527–532.
28 B. M. Mohamed Ali, S. F. Gheida, N. A. El Mahdy and S. N. Sadek, *J. Cosmet. Dermatol.*, 2017, **16**, 52–60.
29 R. H. LaMotte, X. Dong and M. Ringkamp, *Nat. Rev. Neurosci.*, 2014, **15**, 19–31.
30 A. Ikoma, M. Steinhoff, S. Stander, G. Yosipovitch and M. Schmelz, *Nat. Rev. Neurosci.*, 2006, **7**, 535–547.
31 X. J. Chen and Y. G. Sun, *Nat. Commun.*, 2020, **11**, 3052.
32 A. M. Schoelermann, K. A. Jung, B. Buck, E. Gronniger and S. Conzelmann, *J. Eur. Acad. Dermatol. Venereol.*, 2016, **30**(Suppl 1), 18–20.
33 J. H. Hong, H. J. Chen, S. J. Xiang, S. W. Cao, B. C. An, S. F. Ruan, B. Zhang, L. D. Weng, H. X. Zhu and Q. Liu, *Pharmacogn. Mag.*, 2018, **14**, 110–115.
34 J. H. Kim, J. A. Ko, J. T. Kim, D. S. Cha, J. H. Cho, H. J. Park and G. H. Shin, *J. Agric. Food Chem.*, 2014, **62**, 725–732.
35 R. G. Roberts, R. A. Westerman, R. E. Widdop, R. R. Kotzmann and R. Payne, *Agents Actions*, 1992, **37**, 53–59.

36 S. K. R. Khambam, M. U. R. Naidu, P. U. Rani and T. R. K. Rao, *Pharmacol. Pharm.*, 2011, **2**, 159.
37 A. D. Guler, A. Rainwater, J. G. Parker, G. L. Jones, E. Argilli, B. R. Arenkiel, M. D. Ehlers, A. Bonci, L. S. Zweifel and R. D. Palmiter, *Nat. Commun.*, 2012, **3**, 746.
38 G. S. Hahn, *Dermatol. Surg.*, 1999, **25**, 689–693.
39 A. D. Papoiu, R. Valdes-Rodriguez, L. A. Nattkemper, Y. H. Chan, G. S. Hahn and G. Yosipovitch, *Acta Derm.-Venereol.*, 2013, **93**, 520–526.
40 E. Lee, S. An, T. R. Lee and H. K. Kim, *Skin. Res. Technol.*, 2009, **15**, 464–469.
41 A. C. Sintov, I. Krymberk, V. Gavrilov and R. Gorodischer, *J. Pharm. Pharmacol.*, 2003, **55**, 911–919.
42 R. Ravula, A. K. Herwadkar, M. J. Abla, J. Little and A. K. Banga, *Drug Dev. Ind. Pharm.*, 2016, **42**, 862–870.
43 A. Uc, W. P. Bishop and K. D. Sanders, *South. Med. J.*, 2000, **93**, 596–598.
44 H. Xu, N. T. Blair and D. E. Clapham, *J. Neurosci.*, 2005, **25**, 8924–8937.
45 A. J. Sami, M. Khalid, T. Jamil, S. Aftab, S. A. Mangat, A. R. Shakoori and S. Iqbal, *Int. J. Biol. Macromol.*, 2018, **108**, 324–332.
46 K. S. Bahjat, *J. Pharm. Sci.*, 1963, **52**, 1006–1007.
47 R. Hamidpour, S. Hamidpour, M. Hamidpour and M. Shahlari, *Int. J. Case. Rep. Imag.*, 2013, **4**, 86–89.
48 A. C. de Groot, *Contact Dermatitis*, 1987, **17**, 26–34.
49 B. Berne and A. M. Ros, *Contact Dermatitis*, 1998, **38**, 61–64.
50 C. Borelli, S. Bielfeldt, S. Borelli, M. Schaller and H. C. Korting, *Int. J. Cosmet. Sci.*, 2011, **33**, 37–43.
51 M. B. Poh-Fitzpatrick, *Clin. Plast. Surg.*, 1992, **19**, 745–751.
52 E. Yoon, A. Babar, M. Choudhary, M. Kutner and N. Pyrsopoulos, *J. Clin. Transl. Hepatol.*, 2016, **4**, 131–142.
53 W. Volkel, T. Colnot, U. M. Schauer, T. H. Broschard and W. Dekant, *Toxicol. Appl. Pharmacol.*, 2006, **216**, 331–338.
54 N. Kaplowitz, *Yale J. Biol. Med.*, 1981, **54**, 497–502.
55 Y. Chen, H. Dong, D. C. Thompson, H. G. Shertzer, D. W. Nebert and V. Vasiliou, *Food Chem. Toxicol.*, 2013, **60**, 38–44.
56 J. R. Mitchell, D. J. Jollow, W. Z. Potter, J. R. Gillette and B. B. Brodie, *J. Pharmacol. Exp. Ther.*, 1973, **187**, 211–217.
57 C. Saito, C. Zwingmann and H. Jaeschke, *Hepatology*, 2010, **51**, 246–254.
58 T. B. Jeong, J. H. Kim, S. H. Kim, S. Lee, S. W. Son, Y. Lim, J. Y. Cho, D. Y. Hwang, K. S. Kim, J. H. Kwak and Y. S. Jung, *Lab. Anim. Res.*, 2019, **35**, 16.
59 A. Ramachandran and H. Jaeschke, *Curr. Opin. Toxicol.*, 2018, **7**, 17–21.
60 H. Jaeschke, G. J. Gores, A. I. Cederbaum, J. A. Hinson, D. Pessayre and J. J. Lemasters, *Toxicol. Sci.*, 2002, **65**, 166–176.
61 A. V. Rawlings and C. R. Harding, *Dermatol. Ther.*, 2004, **17**(Suppl 1), 43–48.
62 M. Cork, *J. Dermatol. Treat.*, 1997, **8**, S7–S13.
63 R. S. N. Tavares, T. P. Tao, I. Maschmeyer, S. S. Maria-Engler, M. Schafer-Korting, A. Winter, C. Zoschke, R. Lauster, U. Marx and L. R. Gaspar, *Int. J. Pharm.*, 2020, **589**, 119788.
64 J. Kuhnl, T. P. Tao, K. Brandmair, S. Gerlach, T. Rings, U. Muller-Vieira, J. Przibilla, C. Genies, C. Jaques-Jamin, A. Schepky, U. Marx, N. J. Hewitt and I. Maschmeyer, *Toxicology*, 2021, **448**, 152637.
65 K. Yang, S. J. Yu, J. S. Lee, H. R. Lee, G. E. Chang, J. Seo, T. Lee, E. Cheong, S. G. Im and S. W. Cho, *Nanoscale*, 2017, **9**, 18737–18752.
66 K. Yang, J. S. Lee, S. Han, Y. Jin, A. N. Cho, G. E. Chang, E. Cheong, J. H. Yang, S. Chung and S. W. Cho, *J. Ind. Eng. Chem.*, 2019, **74**, 148–157.
67 K. Yang, H. Jung, H. R. Lee, J. S. Lee, S. R. Kim, K. Y. Song, E. Cheong, J. Bang, S. G. Im and S. W. Cho, *ACS Nano*, 2014, **8**, 7809–7822.
68 Y. Jin, J. U. Lee, E. Chung, K. Yang, J. Kim, J. W. Kim, J. S. Lee, A. N. Cho, T. Oh, J. H. Lee, S. W. Cho and J. Cheon, *Nano Lett.*, 2019, **19**, 6517–6523.